Energy 269 (2023) 126717

Contents lists available at ScienceDirect

Energy

journal homepage: www.elsevier.com/locate/energy

Neural network and URED observer based fast terminal integral sliding mode control for energy efficient polymer electrolyte membrane fuel cell used in vehicular technologies

Usman Javaid [a], Adeel Mehmood [a], Jamshed Iqbal [b,*], Ali Arshad Uppal [a]

[a] Electrical and Computer Engineering Department, COMSATS University Islamabad, Park Road, Islamabad, 44000, Pakistan
[b] School of Computer Science, Faculty of Science and Engineering, University of Hull, Kingston upon Hull, HU6 7RX, UK

ARTICLE INFO

Keywords:
Fuel cell
Neural network
Oxygen excess ratio
Uniform robust exact differentiator
Fast terminal integral sliding mode control
Vehicular technology

ABSTRACT

In this research work, a Neural Network (NN) and Uniform Robust Exact Differentiator (URED) observer-based Fast Terminal Integral Sliding Mode Control (FTISMC) has been proposed for Oxygen Excess Ratio (OER) regulation of a Polymer Electrolyte Membrane Fuel Cell (PEMFC) power systems for vehicular applications. The controller uses URED as an observer for supply manifold pressure estimation. NN is used to estimate the stack temperature which is unavailable. The suggested control method increased the PEMFC's effectiveness and durability while demonstrating the finite-time convergence of system trajectories. By controlling the air-delivery system in the presence of uncertain current requirements and measurement noise, the approach ensures maximum power efficiency. The Lyapunov stability theorem has been used to confirm the stability of the presented algorithm. In addition, the suggested method eliminated the chattering phenomenon and improved power efficiency. Given these noteworthy characteristics, the research has the potential to decrease sensor dependence and production costs while also improving the transient and steady-state response in vehicular applications.

1. Introduction

The depletion of fossil fuels, global warming, strict emission regulations, and rising energy demands have made it difficult to meet the needs of human beings [1]. Although researchers are working on various types of engine oils as in [2], the main problem is the increasing cost of fossil fuels, the environmental impacts associated with them and the limited amount of energy resources [3]. To overcome these energy-related problems, the scientific community is investigating various solutions [4,5]. One of the solutions is to use fuel cells as a power source in vehicular applications [6]. A fuel cell is a device that converts chemical energy into electrical energy through an electrochemical reaction between hydrogen and oxygen [7]. The basic structure of a fuel cell consists of an electrolyte and a catalyst which is sandwiched between the anode and cathode terminals. Fuel cells are used for multiple industrial and commercial applications e.g. stationary and portable applications including transportation [8,9]. One of the most common types of fuel cells that are currently being used in the transportation sector and industries is PEMFC [10]. The use of PEMFCs in automobiles is inspired by the fact that they are lightweight, have high power density with lower operating temperatures, have fast startup time and have zero emissions [11]. These properties render PEMFCs a suitable candidate to be used in small scale vehicles as compared to the other renewable energy sources.

In PEMFC hydrogen is fed through the anode terminal and the Oxygen is fed at the cathode terminal [12]. The electrolyte membrane facilitates the exchange of positive charge carriers, and the electrical load connected to the anode and cathode terminals allows the negative charge carriers to complete their conduction cycle [13]. With changes in altitude, temperature, and partial pressures of the reactant gases at anode and cathode manifolds, PEMFCs' non-linear properties affect the power system's performance and efficiency [14]. If these variations are not addressed they might eventually lead to significant power loss and permanent damage to the fuel cell [15]. Therefore, a non-linear control technique must be used for enhanced performance to maintain the PEMFC's operation at maximum power efficiency. To ensure that the fuel cell powered vehicle has maximum efficiency and extended operational life, a number of PEMFC subsystems need special care. A humidity control system, an air delivery system, a temperature control system, and a power control system are among the subsystems [16]. However, this research work focuses on the control of the air-delivery

* Corresponding author.
E-mail addresses: j.iqbal@hull.ac.uk, iqbal.jam@gmail.com (J. Iqbal).

https://doi.org/10.1016/j.energy.2023.126717
Received 18 April 2022; Received in revised form 12 January 2023; Accepted 13 January 2023
Available online 14 January 2023

system. The fuel cell requires inputs of oxygen and hydrogen. The purest form of hydrogen is used to be used as fuel. A specially made high-pressure carbon fiber tank is used to store the hydrogen for use in vehicles, and air from the atmosphere is used to feed the cell stack with the aid of a compressor to meet the cell stack's oxygen needs. While the OER is the performance parameter, the voltage and power are the outputs that are used to drive the actuators of the vehicle. The task of the air-delivery system is to control the amount of oxygen delivered to the fuel cell [17]. In other words, the air delivery system makes sure that the oxygen excess ratio (OER) is regulated. OER is the proportion of oxygen supplied to oxygen used by the fuel cell during the electrochemical reaction. It has been reported that OER must be kept at a value of 2 for the best power efficiency [18].

2. Literature review

A regulated OER ensures that the membrane of the fuel cell will not suffer from oxygen starvation or flooding. Oxygen starvation can lead to spotting phenomena in the membrane surface resulting in irreversible damage and thus decreasing the efficiency of the PEMFC for the rest of its life span [19]. To regulate the OER, different control approaches have been suggested. For example, researchers have developed different mathematical models of the PEMFC system for its parameter estimation and to design control laws. In literature, third to sixth order mathematical models are available to be used for control design [20–23]. Although the process of order reduction and linearization reduce mathematical complexity, however, it comes at the cost of reduced system accuracy. The ninth order state-space model which was originally developed by Pukrushpan et al. is considered to be the most detailed as well as accurate [24]. Researchers have investigated model-based control strategies for OER regulation like model predictive control [25], first-order and higher-order sliding mode control techniques [26,27]. While on the other hand, model-less control strategies have also been used for OER regulation. For example, intelligent control techniques using neural networks for performance optimization and autonomous vehicle driving [28], fuzzy logic controller [29], super twisting algorithm [30]. Model-less control techniques have various disadvantages when compared to model-based techniques, for example, the fuzzy logic-based control technique ignores the structural properties associated with the physical systems and high computational cost [31,32]. However, massive amounts of training data are needed when using artificial intelligence-based control mechanisms like neural networks. It is crucial to feed the network data from actual plants when training it. Off-line training also requires a sizable data set and high computational requirements. They offer quick response times for real-time applications like vehicular technologies, where the system may be exposed to various uncertainties due to sudden changes in current requirements [33].

In recent years, many observer-based techniques have also been investigated to control the air-delivery system of the PEMFC [19,34]. Kalman filters have been used for state estimation [35]. Reduced-order models have been used in observer-based control design for OER regulation [36]. An adaptive observer has also been developed for state estimation of PEMFC but the drawback of this technique is the lack of robustness against measurement noise [37]. A higher-order sliding mode-based observer has been implemented which is capable of finite-time state estimation [29]. Due to its finite-time convergence in state estimation, independence of the system's initial conditions, and the absence of noise ripples in its derivatives, the uniform robust exact differentiator (URED) has attracted a lot of attention. In spite of the initial conditions of the differentiation error, the URED is designed using a modification to the super twisting algorithm and it comprises high-degree terms that provide exact and finite-time convergence to the input signal derivatives [38]. URED is capable of suppressing oscillations in the system as well as it can be successfully used to reconstruct measured signals [39]. Therefore, the dependence on sensor requirements will be reduced along with the production cost without a trade-off in the accuracy and efficiency of the system when URED based observer is employed for the control of PEMFC in vehicular applications.

The impact of stack temperature is typically ignored in most of the studies. However, the temperature in PEMFC stacks is not uniform, as opposed to a single cell. Therefore, for accurate results, it is crucial to define the stack temperature. The coolant inlet or outlet temperature, or the average of the two, may be used as the stack temperature because it is not possible to measure the stack temperature directly inside the stack. The temperature of the stack can vary by up to 5 K from the inlet to the outlet during measurement [40]. This emphasizes the necessity of specifying the location of temperature sensors in order to obtain comparable results. The temperature has a significant impact on the membranes' level of humidification and, consequently, on the conductivity of protons. As the stack temperature varies during the fuel cell operation and it also changes when measured from inlet and outlet the placement of the temperature sensor is critical. In this situation, a neural network can be very useful in accurately predicting the stack temperature. Neural networks have been shown to be effective at modeling complex systems and can be used to predict various variables in PEMFCs, including temperature [41,42]. In particular, NNs have been used to model the relationship between temperature and other variables such as current density, gas flow rate, and humidity [43]. This allows for the development of control strategies that can maintain desired temperature and humidity levels and improve the overall performance and efficiency of PEMFCs [44]. However, there are also challenges associated with the use of NNs for PEMFC temperature control, such as the need for extensive training data and the risk of over-fitting. Overall, the use of neural networks in PEMFC temperature control shows promise, but further research is needed to fully understand their potential and limitations.

This research presents the design of a novel FTISMC, which is specifically designed to regulate the OER in PEMFCs. The controller uses an observer based on URED to estimate the supply manifold pressure and a NN to estimate the stack temperature, both of which are unmeasured states necessary for controller synthesis. The resulting methodology has been shown to achieve desired performance with finite time convergence. In addition, FTISMC inherits the beneficial properties of sliding mode control, including disturbance rejection, and improved tracking performance [45], making it well-suited for the highly nonlinear PEMFC system. The design of the NN-URED-FTISMC controller is illustrated in Fig. 1. The novelty of the proposed work lies in the inclusion of the stack temperature in the mathematical model of the PEMFC, which was previously ignored in our earlier research [46,47]. Furthermore, one of the unique aspects of this work is the use of a neural network to accurately estimate the variations in stack temperature, which can have significant effects on the performance of the PEMFC due to temperature fluctuations. The stack temperature does not remains constant while reactants flow from the anode to the cathode. By using the estimated temperature in the controller, we aim to mitigate these performance impacts.

The main contributions of this research work are:

- The mathematical model of the PEMFC is revised and now includes the effect of stack temperature.
- A novel NN-URED-FTISMC methodology has been proposed to control the OER of a PEMFC which will optimize the vehicle performance in the presence of measurement noise.
- The stability of FTISMC has been proved using the Lyapunov theorem.
- A URED based state estimation technique has been designed to estimate supply manifold pressure of PEMFC in vehicular applications to reduce sensor requirements and production costs.
- NN has been used as an estimator for the unmeasurable state of stack temperature.
- Robustness of the proposed control technique has been evaluated under sudden current variations for various uncertain conditions in the presence of measurement noise.

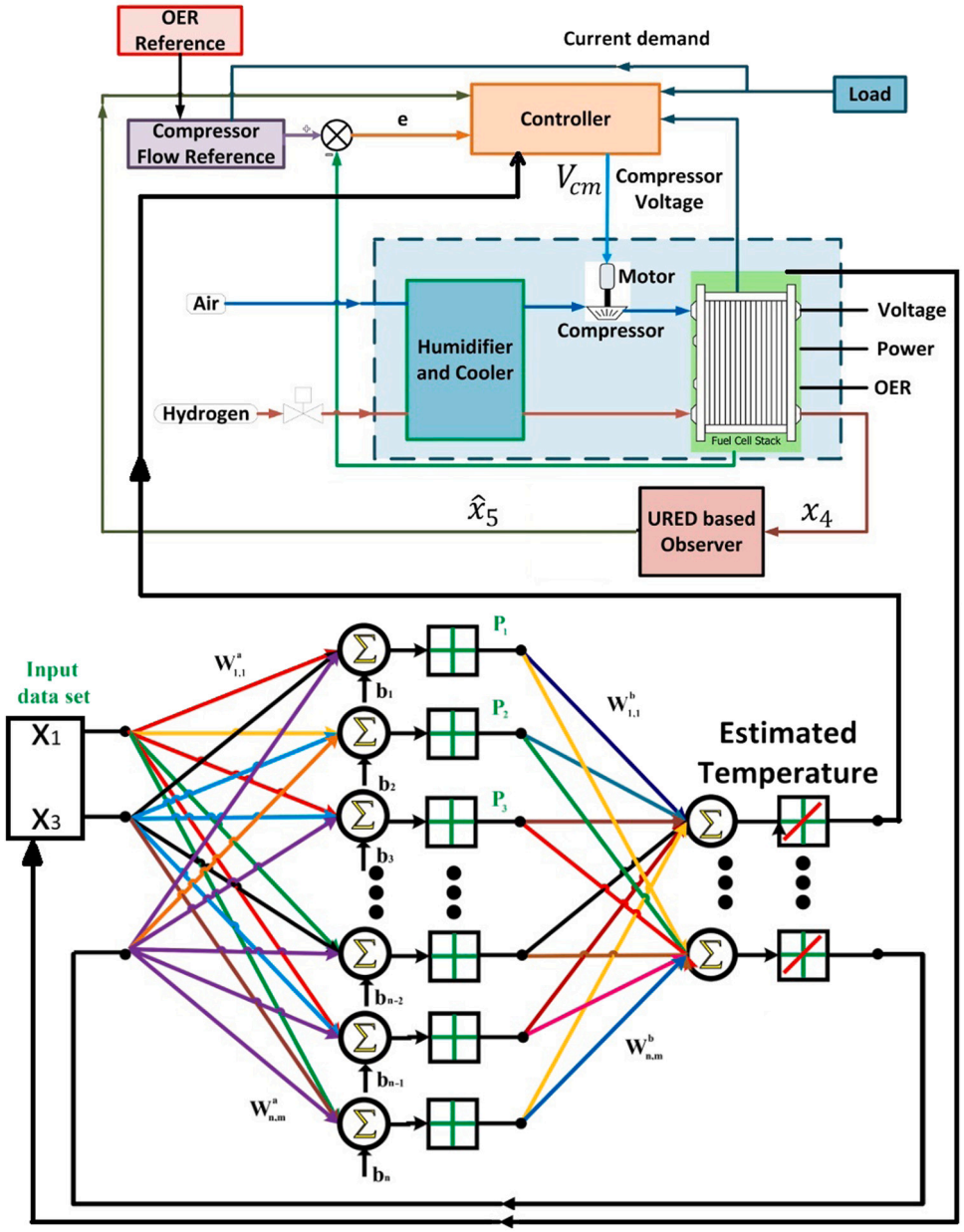

Fig. 1. Control topology for URED FTISMC to control the Air-delivery of PEMFC.

3. Mathematical model of PEMFC

An inlet control valve that regulates the amount of hydrogen fed to the fuel cell stack's anode makes up the PEMFC's air-delivery system. On the other hand, the mass and pressure of the oxygen that is fed at the cathode terminal are controlled by a compressor motor. Instead of using pure oxygen, regular atmospheric air is given to the compressor because doing so would eliminate the need for an additional oxygen tank. A hydrogen tank is used to store the compressed liquid hydrogen in its purest form which will be fed to the PEMFC stack. The compressor motor uses atmospheric air to fulfill the oxygen requirements of the stack. The amount of water vapor content and the temperature of the reactants are controlled by a humidifier and a cooler, respectively. To make sure that the stack moisture stays at a certain level, a water separator is used. To maintain the necessary water level that is feeding the humidifier, it is connected to the water tank. Through the exhaust port, the excess water vapor content is expelled from the car. Reactants are fed into the fuel cell stack, which generates electricity for the traction motors that move the vehicle forward. A radiator is used to control the operating temperature of the fuel cell stack.

There are various mathematical models of PEMFC, for example, some multi-dimensional models have been reported [48,49]. A third-order plant has been used in [50] and a reduced fourth-order model has been used in [21]. All of these reduced-order mathematical models are limited in use because unfortunately, they are not 100% accurate. Therefore, in this research work, the actual ninth-order plant that was originally developed by Pukrushpan et al. is considered to be the most detailed and accurate owing to its accurate and comprehensive nature. After defining the functions F_1–F_{10} to reduce the visual complexity, the state equations of the model can be given by the following set of equations. It has been reported in [51] that stack temperature affects the performance of the PEMFC. The state for stack temperature has been added to the model [52,53]. The modified state space model is given as follows:

$$\dot{x}_1 = a_1 F_1 F_2 F_5 - \left[(F_3)\left(F_3 + (1 - F_3) \times M_{N_2} \right)^{-1} F_4 \left[F_6 \right]^{-1} \right] - a_{11} I_{st} \quad (1)$$

Table 1
Functions F_1–F_{10} used in state space modeling.

$F_1 = \left[1 + \frac{a_2 a_4}{x_5 - x_5 a_{10} + a_3}\right]^{-1}$	$F_2 = k_{sm,out}(x_5 - a_6 x_1 - a_7 x_3 - a_8 m_{v,ca})$
$F_3 = \frac{a_6 M_{O_2} x_1}{a_6 x_1 + a_7 x_3}$	$F_4 = k_{ca,out}(a_6 x_1 + a_7 x_3 + a_8 m_{v,ca} - x_9)$
$F_5 = \left(1 + \frac{a_9 a_{10} x_5}{x_5 - x_5 a_{10}}\right)^{-1}\left(1 + \frac{a_9 a_5}{x_5 - a_{10} x_5}\right)$	$F_6 = 1 + \left(\frac{M_v a_8 m_{v,ca}}{a_6 x_1 + a_7 x_3}\right) \times \left(F_3 + M_{N_2}(1 - F_3)\right)^{-1}$
$F_7 = \frac{a_{23}}{x_4^2}[(\frac{x_5}{p_{atm}})^{a_{24}} - 1] - \beta$	$F_8 = (\frac{x_5}{p_{atm}})^{a_{24}} - 1$
$F_9 = (k_1 k_2 x_5 - k_1 a_{15} x_2 - k_1 a_{14} m_{v,an})$	$F_{10} = \left(\frac{2n_{st}\epsilon_{st}}{M_{st}C_{st}} + \ln[\frac{\sqrt{p_{O_2} p_{H_2}}}{p_{v,hm}}]\frac{x_{10} R n_{st}}{M_{st} C_{st} F}\right)$

The exact values for the variables that have been used in this manuscript are defined in [24].

$$\dot{x}_2 = \left(1 + \frac{a_{12}a_{13}}{a_{15}x_2 + a_{14}m_{v,an}}\right)^{-1}[k_1 k_2 x_5 - k_1 a_{15} x_2 - k_1 a_{14} m_{v,an}] - a_{16} I_{st} \quad (2)$$

$$\dot{x}_3 = (1 - a_1)F_1 F_2 F_5 - \left[1 - \left[(F_3)\left(F_3 + (1 - F_3)M_{N_2}\right)^{-1}\right]F_4\left[F_6\right]^{-1}\right] \quad (3)$$

$$\dot{x}_4 = \frac{a_{25}u^2}{x_4} - a_{26}u - a_{27}\left[(\frac{x_5}{p_{atm}})^{a_{24}} - 1\right] \times \left[a_{22}x_4 - a_{22}x_4 e^{F_7}\right] \quad (4)$$

$$\dot{x}_5 = a_{29}a_{22}x_4\left[1 + \frac{1}{\eta_{cp}}\left[F_8\right]\right] - e^{F_7} - \left[\frac{e^{F_7}}{\eta_{cp}}F_8\right] - \frac{a_{30}x_5}{x_6 k_{sm,out}}F_2 \quad (5)$$

$$\dot{x}_6 = a_{22}x_4 - a_{22}x_4 e^{F_7} - F_2 \quad (6)$$

$$\dot{x}_7 = \left[1 - (1 + \frac{a_{12}a_{13}}{a_{15}x_2 + a_{14}m_{v,an}})^{-1}\right]F_9 - [a_{19}I_{st} - a_{20}(\lambda_{ca} - \lambda_{an})] \quad (7)$$

$$\dot{x}_8 = \left(1 - F_1\right)\left[F_2 F_5 - F_4\left(1 - \left(F_6\right)^{-1}\right]\right] \quad (8)$$

$$\dot{x}_9 = a_{31}[F_4 - W_{rm,out}] \quad (9)$$

$$\dot{x}_{10} = x_{10} + T_{atm}(\frac{-h_s n_{st} A_{sc}}{M_{st}C_{st}}) - F_{10} \quad (10)$$

The Eqs. (11)–(16) describe the input, output, and performance variables;

$$\dot{x} = f(x, u, w) \quad (11)$$

$$x = [m_{O_2} \;\; m_{N_2} \;\; m_{H_2} \;\; \omega_{cp} \;\; p_{sm} \;\; m_{sm} \;\; m_{w_{an}} \;\; m_{w_{ca}} \;\; p_{rm} \;\; T_{st}] \quad (12)$$

$$u = V_{cm} \quad (13)$$

$$w = I_{st} \quad (14)$$

The PEMFC system's output comprises compressor flow, pressure at the supply manifold, and stack voltage(see Table 1).

$$y = [W_{cp} \;\; p_{sm} \;\; V_{st}] \quad (15)$$

The stack voltage, OER and the net power produced by the fuel cell are the performance variables.

$$z = [P_{net} \;\; \lambda_{O_2} \;\; V_{st}] \quad (16)$$

The variables involved in the state space equations are as follows.

$$\lambda_m = \begin{cases} 0.043 + 17.81a_i - 39.85a_i^2 + 36a_i^2 & 0 < a_i \leq 1 \\ 14 + 1.4(a_i - 1) & 1 < a_i \leq 3 \end{cases}$$

and also,

$$W_{rm,out} = a_{32}x_9\left(\frac{p_{atm}}{x_9}\right)^{\frac{1}{2}}\left[\frac{2\gamma}{\gamma - 1}\left[1 - (\frac{p_{atm}}{x_9})^{\frac{\gamma-1}{\gamma}}\right]\right]^{\frac{1}{2}} for \; \frac{p_{atm}}{x_9} > \left(\frac{2}{\gamma + 1}\right)^{\frac{\gamma}{\gamma-1}} \quad (17)$$

Table 2
Coefficients defined in the fuel cell model.

$a_1 = x_{O_{2,ca,in}}$	$a_2 = \frac{M_v}{M_{a,ca,in}}$	$a_3 = \phi^{des} p_{sat,T_{cl}} - a_{13}$	$a_4 = \phi_{ca,in} p_{sat,T_{cl}}$
$a_5 = \phi^{des} p_{sat,T_{cl}}$	$a_6 = \frac{R_{O_2} x_{10}}{V_{ca}}$	$a_7 = \frac{R_{N_2} x_{10}}{V_{ca}}$	$a_8 = \frac{R_v x_{10}}{V_{ca}}$
$a_9 = \frac{M_v}{M_a}$	$a_{10} = \frac{\phi_{atm} p_{sat,T_{atm}}}{p_{atm}}$	$a_{11} = \frac{M_{O_2} n}{4F}$	$a_{12} = \frac{M_v}{M_{H_2}}$
$a_{13} = p_{v,ca,in} = \phi_{ca,in} p_{sat,T_{cl}}$	$a_{14} = \frac{R_v x_{10}}{V_{an}}$	$a_{15} = \frac{R_{H_2} x_{10}}{V_{an}}$	$a_{16} = \frac{M_{H_2} n}{2F}$
$a_{17} = \frac{M_v n}{2F}$	$a_{18} = \frac{\rho_{m,dry}}{M_{m,dry}}$	$a_{19} = \frac{n_d}{A_{fc} F}$	$a_{20} = \frac{D_w a_{18}}{t_m}$
$a_{21} = M_v A_{fc} n$	$a_{22} \frac{\phi_{max} \rho \pi d_c^2 \kappa_{n_c} \delta}{4 n^{0.5}}$	$a_{23} = \frac{\beta 2 C_p T_{cp,in}}{K_{n_c}^2 \psi_{max}}$	$a_{24} = \frac{\gamma - 1}{\gamma}$
$a_{25} = \frac{\eta_{cm}}{J_{cp} R_{cm}}$	$a_{26} = \frac{\eta_{cm} k_v}{J_{cp} R_{cm}}$	$a_{27} = \frac{C_p T_{atm}}{e f_{mc} \eta_{cp} J_{cp}}$	$a_{28} = a_{23}(\frac{1}{p_{atm}})^{a_{24}}$
$a_{29} = \frac{\gamma R_a T_{atm}}{V_{sm}}$	$a_{30} = k_{sm,out}\gamma$	$a_{31} = \frac{R_a T_{rm}}{V_{rm}}$	$a_{32} = \frac{C_{D,rm} A_{T,rm}}{\sqrt{R T_{rm}}}$

and

$$W_{rm,out} = a_{32}x_9\gamma^{\frac{1}{2}}\left(\frac{2}{\gamma + 1}\right)^{\frac{\gamma+1}{2(\gamma-1)}} for \; \frac{p_{atm}}{x_9} \leq \left(\frac{2}{\gamma + 1}\right)^{\frac{\gamma}{\gamma-1}} \quad (18)$$

The model coefficients are given in Table 2. The abbreviations are defined in Appendix A.1 and model parameters are given Appendix A.3 [24].

In the fuel cell, Gibbs free energy is converted into electrical energy, if this process becomes reversible. In this case, two moles of electrons will pass through the electrical circuit for every mole of hydrogen and the electric work done will be given as

$$Work Done(Electric) = -2FE \quad (19)$$

If the system is reversible then we can write the equation for Δg_f as

$$\Delta g_f = -2FE \quad (20)$$

The voltage of the fuel cell, when the process is reversible is called the Nernst voltage is given as

$$E = -\frac{\Delta g_f}{2F} = \frac{\Delta g_f^\circ}{2F} + \frac{RT_{fc}}{2F} ln\left[\frac{p_{H_2} p_{O_2}^{0.5}}{p_{H_2O}}\right] \quad (21)$$

The factor $\frac{\Delta g_f^\circ}{2F}$ changes with the temperature and has a difference of $E_o = 1.229$ to its value at standard temperature and pressure and is given as

$$-\frac{\Delta g_f^\circ}{2F} = 1.229 + (T_{fc} - T_o)\left(\frac{\Delta S^o}{2F}\right) \quad (22)$$

Where $T_o = 298.15$ °C. Using standard entropy changes the thermodynamical values in Eq. (22) is further elaborated as in [54].

$$E = 1.229 - 0.85 \times 10^{-5}(T_{fc} - 298.15) + 4.3085 \times 10^{-5} T_{fc}\left[ln(p_{H_2}) + \frac{1}{2}ln(p_{O_2})\right] \quad (23)$$

The current density is given as

$$i = \frac{I_{st}}{A_{fc}} \quad (24)$$

where A_{fc} is the surface area of the fuel cell.

If we consider all voltage losses occurring in a fuel cell the cell voltage is given as in Eq. (25) [55]

$$V_{fc} = E - v_{ohm} - v_{conc} - v_{act} \quad (25)$$

where v_{ohm}, v_{conc} and v_{act} are ohmic, concentration and activation voltage losses given by the following equations:

$$v_{conc} = \left(c_2 \frac{i}{i_{max}}\right)^{c_3} \quad (26)$$

$$v_{act} = aln\frac{i}{i_o} \quad (27)$$

where a and i_o are constants. For the complete range of current activation, voltage loss is given as

$$v_{act} = v_o + v_a(1 - e^{-c_1 i}) \tag{28}$$

The Eq. (29), is valid for $i > i_o$.

$$v_o = 0.279 - 8.5 \times 10^{-4}(T_{fc} - 298.15) + 4.308 \times 10^{-5} T_{fc}\left[ln\left(\frac{p_{ca} - p_{sat}}{1.01325}\right) + \frac{1}{2} ln\left(\frac{0.1173(p_{ca} - p_{sat})}{1.01325}\right)\right] \tag{29}$$

$$v_a = \left(-1.618 \times 10^{-5} T_{fc} + 1.618 \times 10^{-2}\right)\left(\frac{p_{O_2}}{0.1173} + p_{sat}\right)^2 + (1.8 \times 10^{-4} T_{fc} - 0.166)\left(\frac{p_{O_2}}{0.1173} + p_{sat}\right) + (-5.8 \times 10^{-4} T_{fc} + 0.5736) \tag{30}$$

If we substitute the values of v_{ohm}, v_{conc} and v_{act} in Eq. (25) we get Eq. (31)

$$V_{fc} = E - [iR_{ohm}] - \left[i\left(c_2 \frac{i}{i_{max}}\right)^{c_3}\right] - [v_o + v_a(1 - e^{-c_1 i})] \tag{31}$$

Since the fuel cell stack consists of many fuel cells, fuel cell stack voltage can be obtained by multiplying the number of fuel cells n with cell voltage V_{fc} as shown in Eq. (32)

$$V_{st} = nV_{fc} \tag{32}$$

The parameters in the mathematical modeling of the PEMFC stack voltage are given in Table A.8

4. Control objective

The PEMFC serves as a power source when it is used in automobiles. The compressor motor is also powered by the energy generated by the cell stack in addition to the actuator motor, which propels the vehicle. As a result, the fuel cell's net power is equal to the difference between the stack power the fuel cell stack produces and the stack power the compressor motor voltage consumes. It has been reported in [56] that the compressor motor utilizes almost 30% of the power that is being produced by the device. Therefore, the OER is kept at a predetermined optimum value to minimize power losses in the compressor motor, to protect the system from being permanently damaged due to oxygen starvation or flooding, and to ensure that the fuel cell is getting enough fuel. The expression for OER is given by Eq. (33) which is the ratio of the mass of supplied oxygen $W_{O_{2,in}}$ and the reacted oxygen $W_{O_{2,react}}$.

$$\lambda_{O_2} = \frac{W_{O_{2,in}}}{W_{O_{2,react}}} \tag{33}$$

To fulfill the vehicle's electrical requirements the OER should be maintained at $\lambda_{O_2} = 2$ for optimum performance as specified in [57]. Fluctuations in OER can result in non-uniform behavior of compressor flow rate, stack voltage, and power thus compromising the vehicle's performance. Variations in the fuel cell's power output will permanently harm the compressor motor and the actuator motors it drives in the vehicle. Therefore, it is imperative to avoid chattering and fluctuations at all costs. The control goal of this research work is to regulate the OER to the ideal value of 2, which is accomplished by creating an NN-URED-FTISMC.

To employ model-based control strategy for regulating OER to a desired level, it is mandatory to estimate the unmeasured states, which include stack temperature in a cell stack subsystem and supply manifold pressure. The stack temperature can vary between the inlet and outlet, making it difficult to measure accurately. To address this challenge, we have employed a non auto regressive NN as an estimator to predict the unmeasured stack temperature. Additionally, we have utilized a URED-based observer design to estimate the supply manifold pressure, which is another important variable that affects the OER of the system.

The proposed control design shown in Fig. 1 consists of multiple loops. The inner loop provides the compressor flow rate as a feedback signal to the FTISMC controller. The second loop provides the URED observer-based estimated state to the controller. The observer uses compressor motor speed to estimate the supply manifold pressure. State estimation using observer-based architecture reduces the sensor requirement in control design. The stack temperature is not measurable. So a neural network is used in a third feedback loop as an estimator to provide the accurate value of the stack temperature to the controller.

5. Fast terminal integral sliding mode control design

The main difficulty in designing the controller for OER regulation is that it cannot be directly measured. Moreover, it can be observed in relation of OER, the partial pressure of oxygen at the cathode terminal is unavailable. Also, a sensor for compressor speed measurement and the supply manifold pressure measurement for the conventional non-linear controller design is required. So, to regulate the OER compressor flow rate must be controlled and a reference compressor flow rate is defined. The difference between the actual and the desired compressor flow rate is defined as an error. The expression for error can be given as in (34) using the mathematical model of compressor flow dynamics, a reference compressor flow rate which will be required to regulate the OER in the PEMFC can be computed in the following manner

$$e(x,t) = W_{cp} - W_{cp,ref} \tag{34}$$

The compressor flow rate is defined as

$$W_{cp} = \frac{\Psi_{max}\rho_a \pi d_c^2 (\frac{\pi}{60} d_c(\omega_{cp}/\sqrt{\theta}))}{4\sqrt{\theta}} \times \left[1 - exp^{\left[\frac{2\beta C_p T_{cp,in}}{(\frac{\pi}{60} d_c(\omega_{cp}/\sqrt{\theta}))^2 \Psi_{max}}\left(\frac{p_{cp,out}}{p_{cp,in}}^{\frac{\gamma-1}{\gamma}} - 1\right) - \beta\right]}\right] \tag{35}$$

By using reference airflow at the cathode terminal, mass flow reference $W_{cp,ref}$ can be found from the oxygen flow reference at the cathode. The required mass flow of dry air can be given by Eq. (36)

$$W_{dry,ref} = \frac{1}{x_{O_2}} W_{O_2,ca,ref} = \frac{1}{x_{O_2}} \lambda_{O_2,ref} M_{O_2} \frac{nI_{st}}{4F} \tag{36}$$

Considering the relative humidity of the air, the required flow rate of air can be given as in Eq. (37)

$$W_{cp,ref} = (1 + \omega_{amb}) \frac{1}{x_{O_2}} \lambda_{O_2,ref} M_{O_2} \frac{nI_{st}}{4F} \tag{37}$$

So if we substitute Eqs. (36) and (37) in (34) the equation for error can be represented as Eq. (38)

$$e(x,t) = \frac{\Psi_{max}\rho_a \pi d_c^2 (\frac{\pi}{60} d_c(\omega_{cp}/\sqrt{\theta}))}{4\sqrt{\theta}} \times \left[1 - exp^{\left[\frac{2\beta C_p T_{cp,in}}{(\frac{\pi}{60} d_c(\omega_{cp}/\sqrt{\theta}))^2 \Psi_{max}}\left(\frac{p_{cp,out}}{p_{cp,in}}^{\frac{\gamma-1}{\gamma}} - 1\right) - \beta\right]}\right] - (1 + \omega_{amb}) \frac{1}{x_{O_2}} \lambda_{O_2,ref} M_{O_2} \frac{nI_{st}}{4F} \tag{38}$$

The sliding surface is defined as

$$s = \alpha e(t) + \beta \int |e|^{\gamma} sign(e) dt \tag{39}$$

The term $|e|^{\gamma}$ in the sliding surface ensures the finite time convergence of the error dynamics. Where $\gamma = p/q$, p and q are positive odd integers. Where the tracking error is defined by the variable e and α, β, γ are used as tuning parameters. While choosing the value of α and β, it must be considered that the Hurwitz condition is satisfied i-e $\alpha > 0$ and $\beta > 0$, Whereas $0 < \gamma < 1$. The time derivative of the Eq. (39) becomes

$$\dot{s} = \alpha \dot{e}(t) + \beta |e|^{\gamma} sign(e) \tag{40}$$

where

$$\dot{e} = \dot{W}_{cp} - \dot{W}_{cp,ref} \tag{41}$$

The strong reach-ability law can be defined by Eq. (42). When implementing this FTISMC, an integral of the error function is added to the equation. The continuous control part is obtained by taking the first-order time derivative of the sliding function and equating it to 0.

$$u_{dis} = -K_1 s - K sign(s) \tag{42}$$

The overall control law is given as

$$u = u_{eq} + u_{dis} \tag{43}$$

The continuous control part is obtained by taking the first-order time derivative of the sliding function and equating it to 0. The term $\dot{e}(t)$ has already been defined in Eq. (41). After substituting the value of $\dot{W}_{cp}$ and $\dot{W}_{cp,ref}$, the first-time derivative of the sliding surface can be written as follows

$$\dot{s} = \alpha(au^2 + bu + c) + \beta|e|^{\gamma} sign(e) \tag{44}$$

Where

$$a = \left[a_{22} - a_{22}e^{F_7} + \frac{2a_{22}a_{23}}{p_{atm}^{a_{24}}} \times e^{F_7}x_5^3x_4^{-2} - 2a_{22}a_{23}e^{F_7}x_4^{-2}\right]c_4x_4^{-1} \tag{45}$$

$$b = -a_{26}\left[a_{22} - a_{22}e^{F_7} + \frac{2a_{22}a_{23}}{p_{atm}^{a_{24}}} \times e^{F_7}x_5^3x_4^{-2} - 2a_{22}a_{23} \times e^{F_7}x_4^{-2}\right] \tag{46}$$

$$\begin{aligned} c = &-\left[a_{22} - a_{22}e^{F_7} + \frac{2a_{22}a_{23}}{p_{atm}^{a_{24}}} \times e^{F_7}x_5^3x_4^{-2} - 2a_{22}a_{23} \times e^{F_7}x_4^{-2}\right] \\ &\frac{a_{27}}{k_{sm,out}}F_2\left[a_{22}x_4 - a_{22}x_4[e^{F_7}]\right] - \left(\frac{a_{22}a_{23}a_{24}e^{F_7}x_4^{-1}x_5^{a_{24}-1}}{p_{atm}^{a_{24}}}\right)\times \\ &\left(a_{29}a_{22}x_4[1 + \frac{1}{\eta_{cp}}F_8]\right) - e^{F_7} - \frac{e^{F_7}}{k_{sm,out}\eta_{cp}}F_2 - a_{30}\frac{x_5}{x_6k_{sm,out}}F_2 \\ &- 2.8 \times 10^{-2}\frac{dI_{st}}{dt} \end{aligned} \tag{47}$$

To reduce the chattering phenomena in FTISMC, saturation functions are used instead of using the simple $sign()$ function in the discontinuous and as-well-as continuous parts of the controller, which is defined as in Eq. (48)

$$sat(s) = \begin{cases} 1 & s \le 0 \\ K & s|s| \le \delta \\ -1 & s \le -\delta \end{cases} \tag{48}$$

5.1. Lyapunov stability analysis of FTISMC

The existence of URED FTISMC can be proved by evaluating the Lyapunov stability as follows;

$$V = \frac{1}{2}S^2 \tag{49}$$

$$\dot{V} = S\dot{S} = S(au^2 + bu + c + (\beta/\alpha)|q|^{\gamma} sign(e)) \tag{50}$$

where

$$u = \frac{-b + \sqrt{b^2 - 4a(c + (\beta/\alpha)|q|^{\gamma} sign(e))}}{2a} - K_1 s - K_2 sign(s) \tag{51}$$

After substituting the value of u in (50) we get

$$\dot{V} = S[0 - K_1 S - K_2 sign(S)]$$

$$\dot{V} \le -S(K_1)S - K_2 S sign(S)$$

$$\dot{V} \le -K_1 S^2 - K_2|S|$$

$\dot{V} \le 0$, $\forall\ K_1 > 0$, $\forall\ K_2 > 0$ For a system to be stable, the rate of change for the Lyapunov function must be negative. The above equations indicate that $\dot{V} \le 0$, $\forall\ K_1 > 0$, $\forall\ K_2 > 0$. Therefore the Lyapunov function is negative definite proving the existence and finite time stability of the sliding mode, considering that $ssign(s) = |s|$

Thus proving finite-time convergence and asymptotic stability, ensuring the existence of URED based FTISMC. The (52) shows the finite time required to reach the sliding surface given as (cf. [58])

$$T_S \le \frac{1}{2\bar{K}_1}\ln\left(\frac{\bar{K}_1V^{1/2}(S(0)) + \bar{K}_2}{\bar{K}_2}\right) \tag{52}$$

6. URED-based observer design

FTISMC is a variant of the SMC technique and is widely accepted to be an effective control technique that is used as a robust control strategy for overcoming the non-linearities of various control-related problems. This family of sliding mode control strategies has an inherited property of finite-time convergence and robustness against internal/external disturbances and uncertainties. The effectiveness of FTISMC has been evaluated for PEMFC air delivery system in [47] which showed better performance than the super twisting algorithm derived in [46]. However, in some cases, faulty sensors can cause incorrect measurement issues. These issues cause problems while calculating the system response in the presence of sudden variations in the operating conditions of the vehicle. In this research work, URED observer is designed for the state x_5 to overcome the issues of faulty sensing networks and matched or unmatched uncertainties due to the measurement noise present in sensing networks. The proposed URED observer design also reduces the system cost by making the system independent from sensor requirements. Therefore a smooth URED observer has been proposed in this research work as a state estimator which will give an estimated value of supply manifold pressure. The proposed URED has the remarkable property of overcoming the high-frequency chattering phenomena and thus improving the overall response of nonlinear systems. Based on the generalized STA the URED is proposed by the following equation [38].

$$\dot{z_0} = -k_1\Phi_1(\sigma_0) + z_1 \tag{53}$$

$$\dot{z_1} = -k_2\Phi_2(\sigma_0) \tag{54}$$

where $\sigma_0 = z_0 - \zeta$ is the estimation error, and k_1 and k_2 are the positive gains. The URED has two states, z_0 defines the actual signal and z_1 is its derivative. $\Phi_1(\sigma_0)$ and $\Phi_2(\sigma_0)$ are characterized as

$$\Phi_1(\sigma_0) = |\sigma_0|^{\frac{1}{2}} sign(\sigma_0) + \mu\sigma_0^{\frac{3}{2}} sign(\sigma_0) \tag{55}$$

$$\Phi_2(\sigma_0) = \frac{1}{2}sign(\sigma_0) + \frac{3}{2}sign(\sigma_0)|\sigma_0|^2 \tag{56}$$

When the sliding mode is established $\dot{z_0} = z_1$ and the uniform derivative is computed. In order to design the URED based observer for x_5 using x_4 we substitute z_1 in the place of $\dot{x_4}$ in the Eq. (4) and get the following equation

$$z_1 = \frac{a_{25}u^2}{x_4} - a_{26}u - a_{27}\left[(\frac{x_5}{p_{atm}})^{a_{24}} - 1\right] \times \left[a_{22}x_4 - a_{22}x_4e^{F_7}\right] \tag{57}$$

The above equation has been solved for the estimated supply manifold pressure $\hat{x_5}$ shown as follows

$$\hat{x_5} = p_{atm}\left[1 + \frac{\left(z_1 - \frac{a_{25}u^2}{x_4} + a_{26}u\right)}{(-a_{27})\left(a_{22}x_4 - a_{22}x_4e^{F_7}\right)}\right]^{\frac{1}{a_{24}}} \tag{58}$$

In the case of PEMFC sudden variation, the demand current creates a sudden surge in all the states of the PEMFC system. This is due to the fact that all the states are inter-coupled and sudden variation in a single parameter produces abrupt changes in all the state parameters. The URED ensures finite-time and theoretical exact convergence of such abrupt changes of the signals whenever their derivatives are Lipschitz [38]. The URED ensures bounded convergence independent of the initial conditions and the differentiation error. The uniform and finite time convergence is ensured by the high-degree terms $\sigma_0^{\frac{3}{2}} sign(\sigma_0)$ and $sign(\sigma_0)|\sigma_0|^2$.

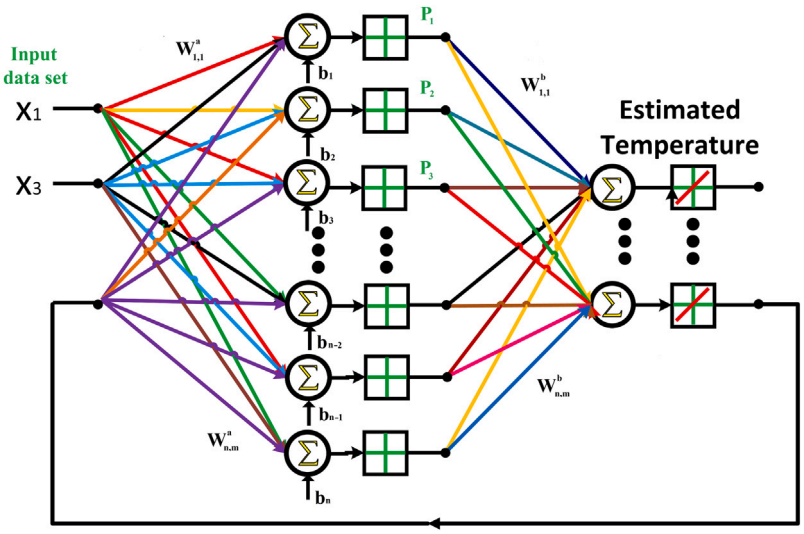

Fig. 2. NN for stack temperature estimation.

7. Non auto regressive NN design for stack temperature estimation

When assessing the dynamic performance of the fuel cell-based system, model-based control laws are extremely important. The primary challenge in developing a controller that uses a sensor-based architecture is that the sensors' accuracy gradually degrades over time. A temperature sensor must be built into the PEMFC in order to measure the precise stack temperature, which can raise the cost of the system. Additionally, temperature sensors that are used for extended periods of time may have slower response times and inaccurate measurements. Using the data from other states, a NN can be used to precisely estimate the stack temperature. Therefore, when designing the NN temperature estimator, model-based system dynamics were taken into account. In this research article, a NN-based method for estimating stack temperature has been suggested. In addition to resolving the issue of slow sensor response times, NN lowers system costs by reducing the number of sensors needed. The proposed control scheme has been depicted in Fig. 1. The actual data of PEMFC plant which is controlled using FTISMC in [47] has been used to train the NN to estimate the stack temperature. The States x_1 and x_3 are used for stack temperature estimation. The reason of using these two particular states is that the state of temperature is related to these particular states by the following two ideal gas equations. Moreover, the data from these two states incorporate the change in temperature from anode to cathode. The Levenberg–Marquardt algorithm has been used in the NN for curve fitting which interpolates between the Gauss–Newton algorithm and the method of gradient descent.

$$T_{st} = \frac{p_{O_{2,ca}} V_{ca}}{m_{O_{2,ca}} R_{O_2}} \tag{59}$$

$$T_{st} = \frac{p_{H_{2,an}} V_{an}}{m_{H_{2,an}} R_{H_2}} \tag{60}$$

For the stack temperature estimation of the PEMFC, the non auto regressive NN with exogenous inputs is used. As the state of stack temperature is dependent on its previous value. Therefore the mentioned NN is preferred as it has a feedback state. The NN has to be trained initially. The training process is completed by mapping input data to the output data of the PEMFC. Once the NN training process is complete, the trained network is then used to estimate the output signal. The trained NN will provide the estimated output according to the input conditions provided by the user. The training method of the NN adopts optimization algorithms that use either jacobians or gradients to complete the task at hand. The states x_1 and x_3 of the PEMFC are acting as the inputs to the NN, whereas the estimated stack temperature is the output of the NN. The generalized equations given as (61) and (62) are used for the feed forward NN to generate the estimated control signal T_{est}.

$$P_N = \mathcal{F}_N^1\left(\sum_{n=1}^{N} W_{N,n}^1 X + b_N^1\right) = \mathcal{F}_N^1\left(\boldsymbol{W}_N^{1^T} \boldsymbol{X}_n + b_N^1\right), \tag{61}$$

$$\hat{T}_{est} = \mathcal{F}_m^2\left(\sum_{N=1}^{m} \hat{W}_{T_{est},N}^2 P_N\right) = \hat{\boldsymbol{W}}_{T_{est}}^{2^T} \boldsymbol{P}_N \tag{62}$$

Where T_{est} is the estimated stack temperature. The generalized diagram of the feed-forward NN for the estimation of control stack temperature is shown in Fig. 2. Where the number of inputs provided to the NN is defined as $n = 50$, and the number of network outputs is $m = 1$ which is the estimated control signal. The second output shown in the figure is the delayed version of the output, used by the NN to predict future values. Here $N = 10$ shows the numbers of hidden layer neurons, and $M = 1$ represents the numbers of output layer neurons. The inputs are $\boldsymbol{X} = [m_{O_2}\ m_{H_2}]^T \in \mathbb{R}^n$ is the input vector of the NN. $\boldsymbol{P}_N \in \mathbb{R}^N$ is the hidden layer output vector, $\boldsymbol{W}_N^1 \in \mathbb{R}^n$ is the hidden-layer weights vector, $\boldsymbol{W}_{U_{est}}^2 \in \mathbb{R}^N$ is the output-layer weights vector and $b^1 \in \mathbb{R}^N$ is the network's bias that are used to increase the learning speed during the network training. In addition, $\mathcal{F}_N^1 : \mathbb{R}^n \to \mathbb{R}^N$ and $\mathcal{F}_m^2 : \mathbb{R}^M \to \mathbb{R}^m$ is the tan-sigmoid function and pure-linear activation functions of hidden layer and output layer neuron, respectively. These functions are used to ensure the best performance during the NN training process.

The output function of the proposed NN design is expressed by the following algorithm

$$T_{est} = \boldsymbol{W}_{T_{est}}^{2^T} \boldsymbol{P} + e_T \tag{63}$$

where e_T is the network approximation error.

The next section of this manuscript presents the results of our simulations and engages in a thorough discussion of their implications. The findings of the comparative study provide a detailed analysis of what they mean for our original hypotheses.

8. Results and discussion

This section elaborates on the performance of the proposed NN-URED-FTISMC technique. The simulations are conducted in MATLAB/Simulink environment to analyze the performance of the FTISMC and NN-URED-FTISMC to observe controllers' behavior. Various performance parameters of the PEMFC including OER, stack voltage and

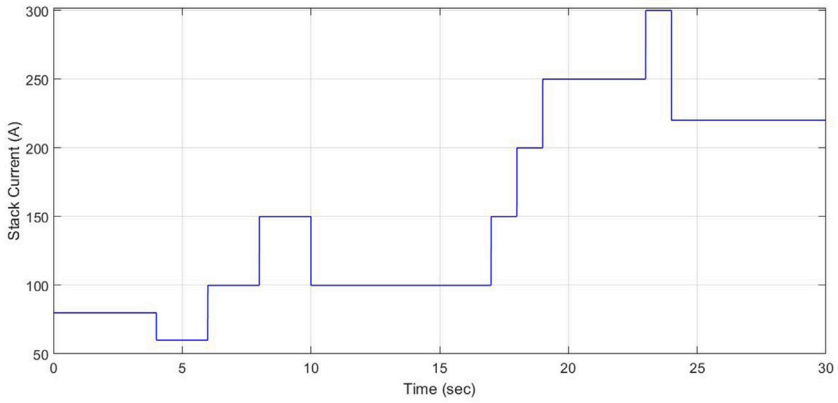

Fig. 3. PEMFC Stack current.

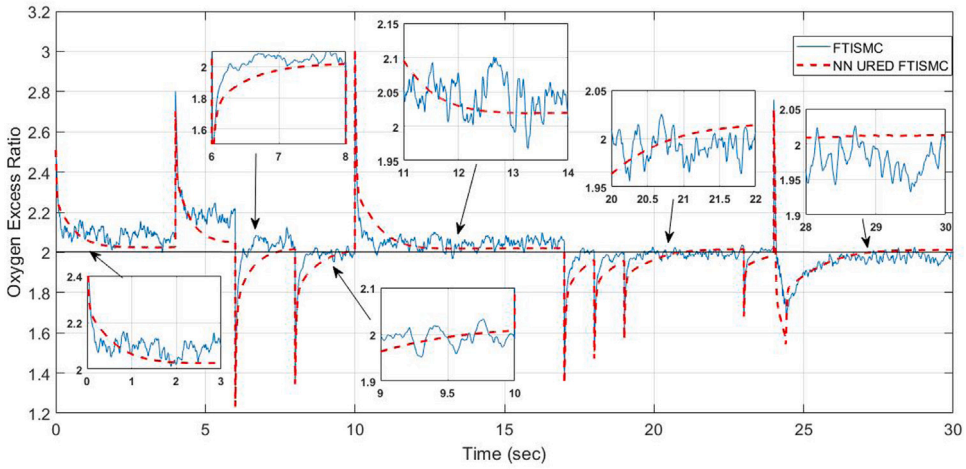

Fig. 4. PEMFC oxygen excess ratio.

power in the presence of model uncertainties and disturbances and measurement noise in compressor speed and supply manifold pressure, along with transient power demands. A current signal which ranges between 60 A to 300 A shown in Fig. 3 is considered as disturbance input which is demanded by the PEMFC-powered vehicular application where the current demand increases or decreases depending upon the requirements of the vehicle. Transient current demands need the amount of the supplied reactants to be adjusted accordingly. Hydrogen is considered to be pre-regulated whereas the amount of oxygen is regulated by the compressor motor speed which in-turn is controlled by the compressor motor voltage. Regulated supply of reactants ensure smooth operation in transient current demands and also protects the membrane from getting it damaged, permanently. Smooth power delivery will ensure the longevity of the actuator motors of the vehicle.

The Fig. 4 depicts the graph of OER. It can be observed that the FTISMC has a lot of fluctuations in the presence of measurement noise. Fluctuations in OER can cause severe damage to the fuel cell membrane which is costly to repair. However, with NN-URED-FTISMC the fluctuations are removed and thus enhancing the life span and maintenance cost of the PEMFC by reducing the requirement of sensors and overcoming the effects of measurement noise without any compromise in system efficiency.

Fig. 5 shows the error tracking of the proposed design with NN-URED-FTISMC and FTISMC. This error signal is the difference between the actual compressor flow rate and the reference compressor flow rate. The reference compressor flow rate is a predefined flow rate which ensures that the OER remain at the specified value. It can be concluded that NN-URED-FTISMC has better performance in terms of error tracking in the presence of measurement noise.

The signal of the compressor motor voltage is given in Fig. 6. The voltage signal is responsible for regulating the supply of oxygen to the fuel cell stack so that the electrochemical reaction can produce the maximum required current and the PEMFC can operate at maximum efficiency ensuring that the OER is maintained at a level of two. It can be observed that in the system where NN-URED-FTISMC is used for the state estimation of compressor speed and supply manifold pressure there is no chattering phenomenon. Whereas, the FTISMC does not completely eliminate the undesirable clattering phenomenon in the presence of wide band measurement noise. Removal of chattering ensures less power consumption by the compressor and smooth operation of PEMFC power system. Observer based control will increase the compressor motor life by ensuring chattering removal and thus reducing operational cost by increasing maintenance time intervals. Fig. 6 shows the control signals for FTISMC and NN-URED-FTISMC. The results show that in the system where URED observer is used for state estimation for compressor speed and supply manifold pressure the control effort is lesser as compared to the system wit FTISMC. Thus it can be concluded that in the presence of measurement noise the NN-URED-FTISMC outperforms the FTISMC. The chattering in the control signal which is being coupled with the compressor motor voltage will be causing severe damage to the motor and will hinder smooth operation of the PEMFC power system. Moreover this type of chattering

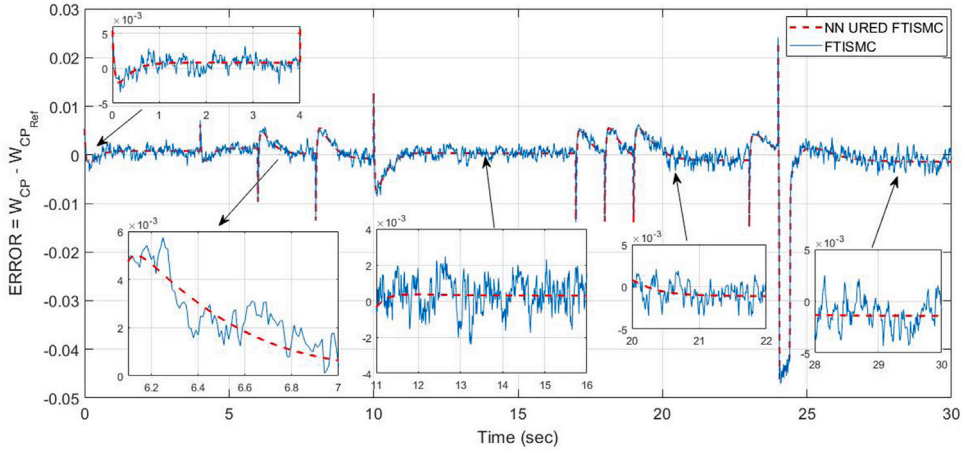

Fig. 5. Error tracking.

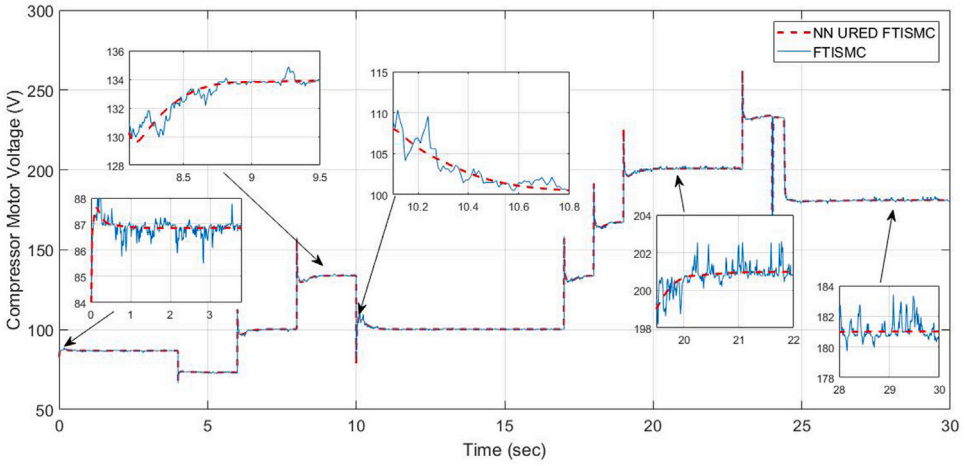

Fig. 6. PEMFC compressor motor voltage.

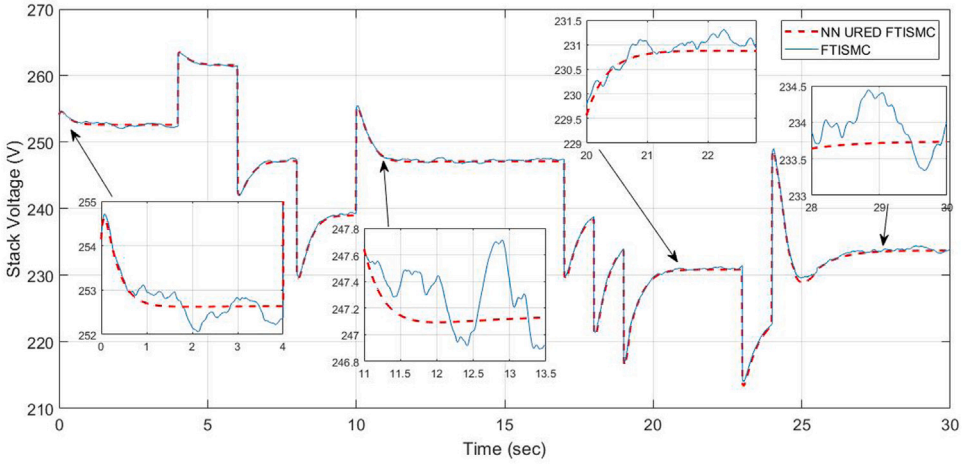

Fig. 7. PEMFC stack voltage.

will damage the traction motors of the vehicle that are being driven with the fuel cell.

The behavior of stack voltage produced by the PEMFC power system is shown in Fig. 7. It is clear form the figure that when NN-URED-FTISMC is used the chattering effect is removed where as the system with FTISMC has significant chattering phenomenon which occurs due to the presence of measurement noise in the states of compressor speed and supply manifold pressure. Chattering free voltage signal ensures that the vehicular application that is being operated by that signal will not be damaged. Moreover observer based control law will reduce the system maintenance cost by avoiding power fluctuations without compromising system efficiency.

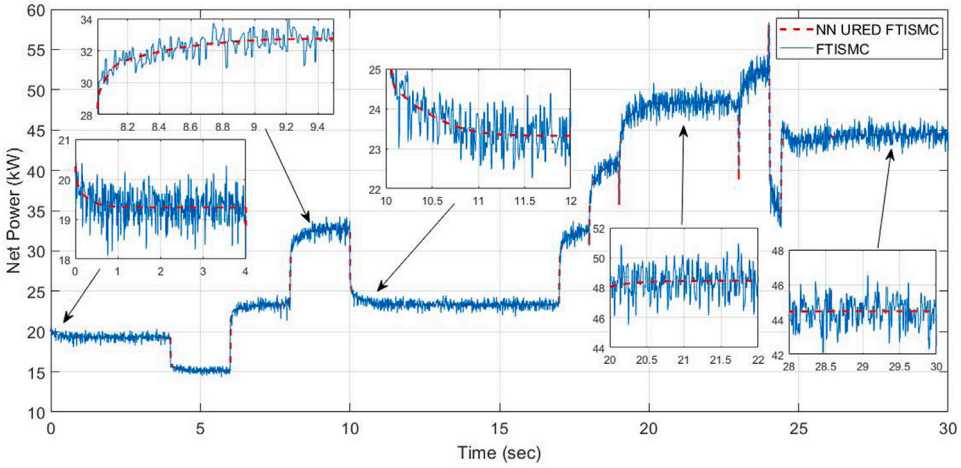

Fig. 8. PEMFC net power.

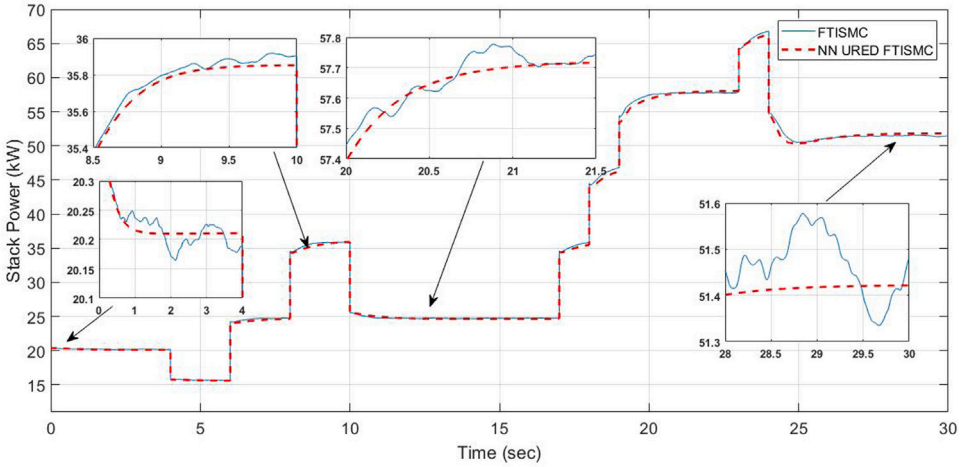

Fig. 9. PEMFC stack power.

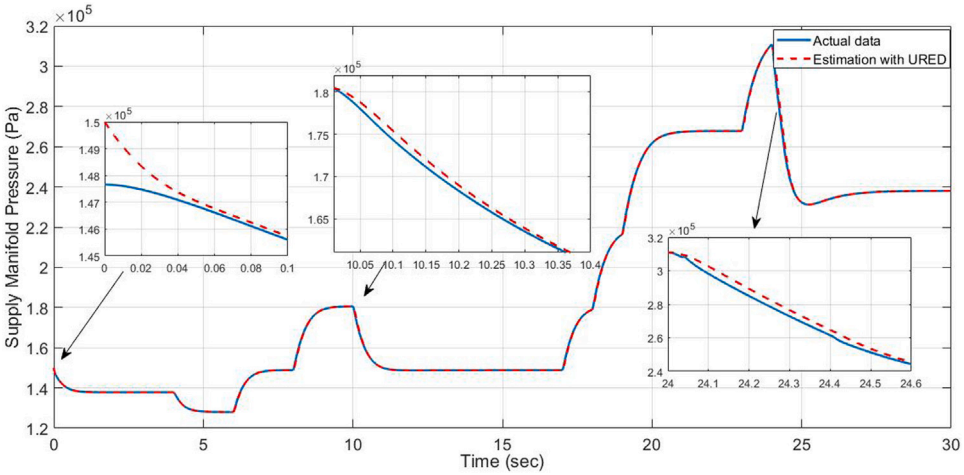

Fig. 10. Supply manifold pressure.

The compressor motor consumes 30% of the total power that is being produced by the PEMFC power system and it acts like a primary load to the system [56]. So the net power that is being produced by the PEMFC power system is the difference between the power being produced by the PEMFC stack and the power consumed by the compressor motor. In Fig. 8 it can be seen that NN-URED-FTISMC scheme has no chattering when the system is exposed to measurement noise in compressor speed and supply manifold pressure. The behavior of stack power is shown in Fig. 9. Therefore it can be concluded that when NN-URED observer based intelligent controller will be used

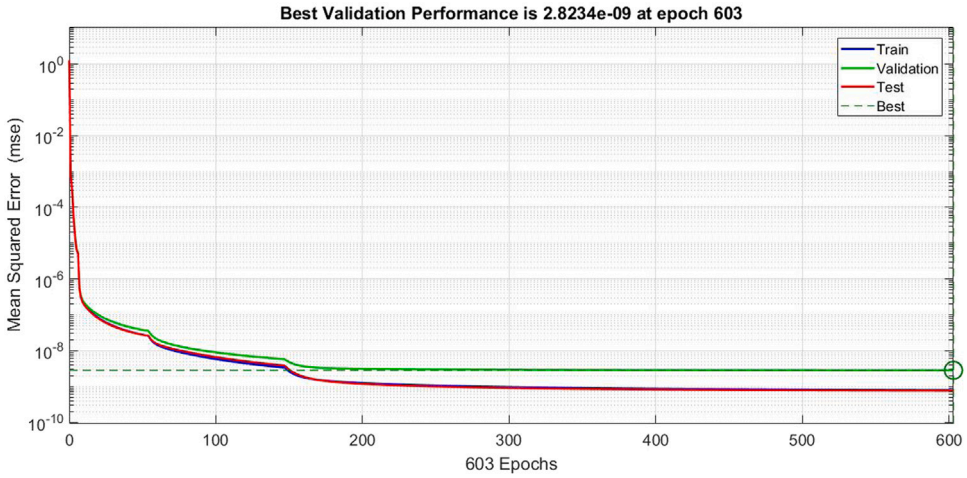

Fig. 11. NN best validation performance.

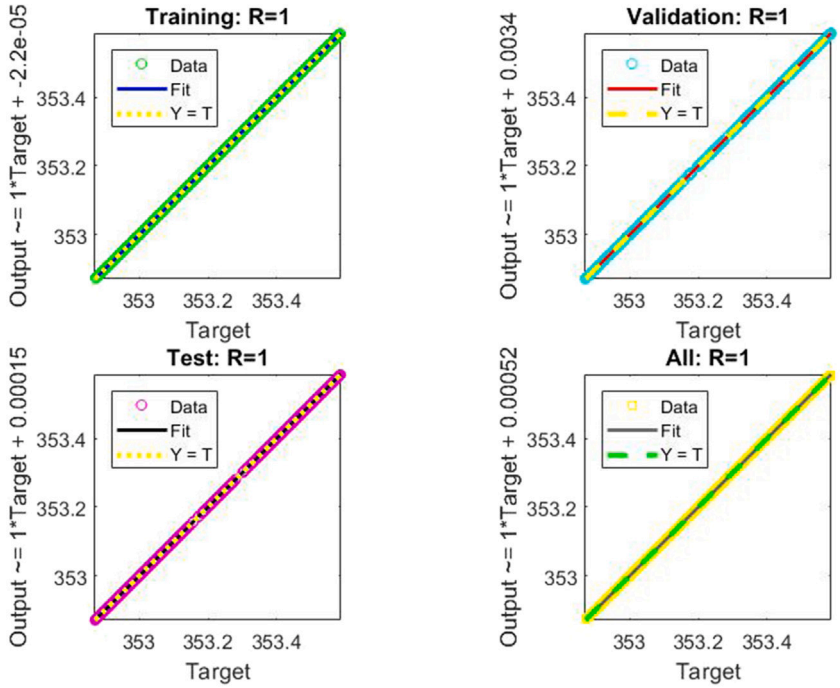

Fig. 12. Regression plot of stack temperature estimation.

to control the PEMFC powered vehicle it will ensure smooth power delivery ensuring the increased life span of the actuator motors and the PEMFC power system. Moreover the use of observer based control reduces the system cost by making the system less dependent upon sensing networks.

The Fig. 10 shows the performance of the proposed URED observer. The zoomed versions of the traces indicate that the proposed observer ensures finite time convergence of the estimated signal regardless to the initial conditions of the system. It can be clearly seen that the URED shows remarkable state estimation regardless of the initial condition with convergence time less than 0.4 s.

Now, the performance of the three-layered non auto regressive NN is explained. One or more batches tend to form an epoch, where a part of the provided data set is utilized to train the NN. The trained NN indicates the performance in terms of error with the best performance error of $2.823e^{-9}$ at 603 epochs. The best validation performance of the NN is shown in Fig. 11.

The regression plot of a NN indicates how accurately the estimation has been made. The plots represent the testing data-set and its validation. The value of R is an indication of the relationship or similarity index between the outputs and target data-set. If the value of $R = 1$, it indicates that there is a perfect match between outputs and target data-set. If the value of R is close to zero, then there is almost no match between the outputs and target data-set. The curve in Fig. 12 implies that the training data has a good fit for stack temperature estimation.

Once the training of the NN is complete the error histogram can be obtained. On the horizontal axis, the plot of the error histogram represents the errors between the target data-set values and predicted values. The errors in Fig. 13 depict how the predicted values are deviating from the target output values. The errors to the left half side of the *Zero Error* are the negative errors and the right half side represent the positive errors. The vertical bars in the error histogram graph are called the bins. The total error range of the trained NN is divided into 20 bins. The vertical axis is representing the number of sample instances from the provided data-set, which lies in a particular

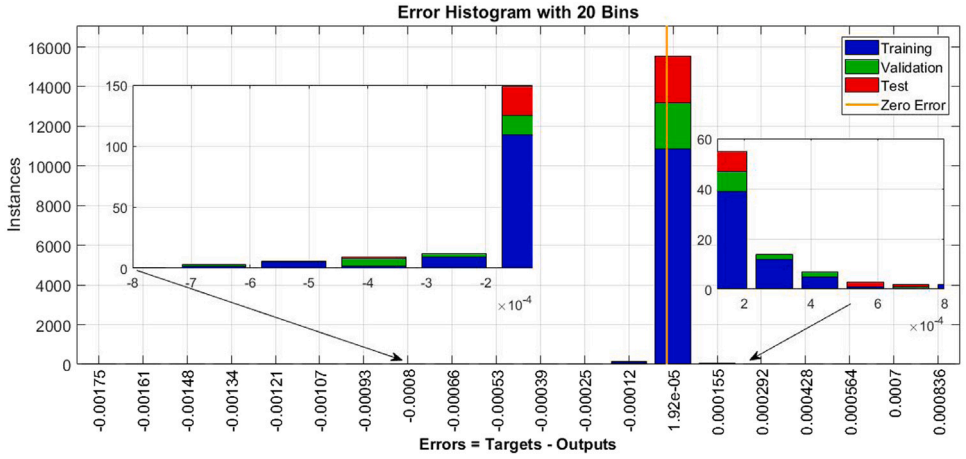

Fig. 13. Error histogram for stack temperature estimation.

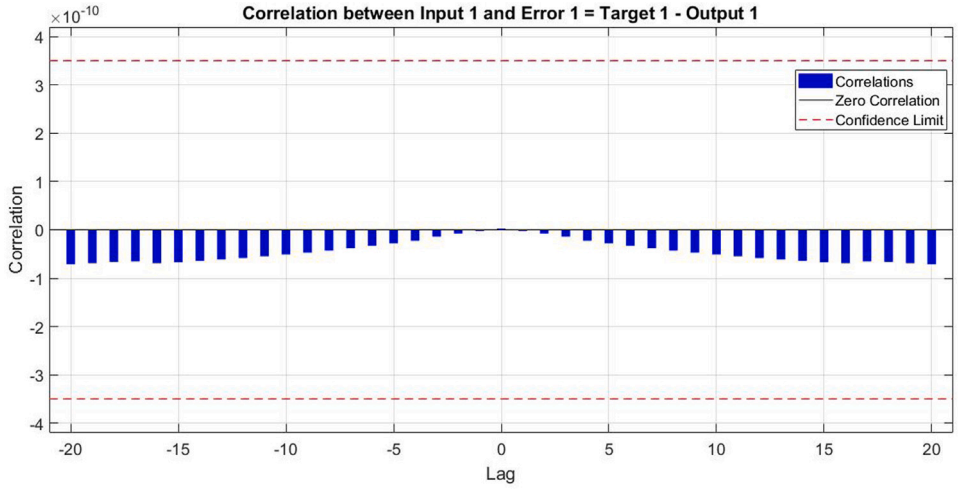

Fig. 14. NN Correlation between input and error.

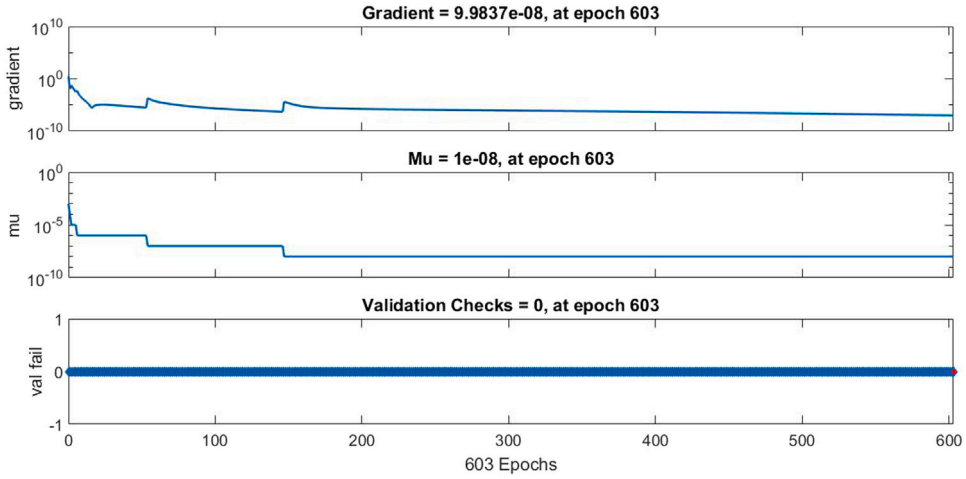

Fig. 15. NN training state.

bin. At the middle of the histogram plot, the bin corresponds to the error of approximately $1.92e^{-5}$, the height of that bin for the training data-set lies below 16 000.

The Fig. 14 shows the Correlations between input and error. Since the ideal model is rarely feasible in practice, 95% confidence intervals around zero are used to assess correlation values. The graph indicates that the correlation lies within the confidence limits.

The training state performance of the NN is shown in Fig. 15 Typically, the goal of training is to minimize the sum of squared errors (gradient) by applying the steepest descent method to optimize the

selection of weights and biases. However, a momentum term is added to slow the descent's speed so that the search value does not repeatedly cross the minimum without stopping close enough to it. The value of gradient is $9.9837e^{-8}$ at 603 epoch. The back propagation process, which updates the neuronal weights, is controlled by the *mu* value during training. The value of *mu* is $1.0e^{-8}$. The validation fail test for he unseen data shows that the NN shows good performance for the unseen data.

9. Conclusion

The objective of this research is the performance improvement of the PEMFC by designing a control law for the air-delivery system. NN-URED-FTISMC has given satisfactory performance in the presence of external disturbances and measurement noise. The simulation results indicate that the proposed methodology effectively maintains the OER in the presence of sudden load variations and measurement noise. This ensures optimum performance and efficiency of the PEMFC. The removal of chattering clearly indicates that the system efficiency is increased. So it can be concluded that NN-URED-FTISMC strategies when used for vehicular applications are capable of reducing system cost by reducing the dependency on sensing networks without reducing the system efficiency and accuracy.

Currently there are certain limitations to the use of fuel cell-based vehicles. There are currently few hydrogen filling stations, PEMFC-based vehicles are not commonly used by the general public. The cost of PEMFC will be lower, and its performance and longevity will be improved, thanks to the material and component advancements, as well as the various optimization and control strategies. By controlling temperature, humidity, and fuel management systems of PEMFCs, future work directions should concentrate on performance and efficiency improvement of PEMFC. This can be achieved by designing and testing various control laws to optimize the performance of various subsystems in fuel cell powered vehicles.

CRediT authorship contribution statement

Usman Javaid: Methodology, Software, Data curation, Writing – original draft. **Adeel Mehmood:** Supervision, Conceptualization, Writing – original draft, Project administration. **Jamshed Iqbal:** Visualization, Investigation, Resources, Writing – review & editing. **Ali Arshad Uppal:** Supervision, Methodology, Formal analysis, Validation.

Declaration of competing interest

The authors declare that they have no known competing financial interests or personal relationships that could have appeared to influence the work reported in this paper.

Data availability

No data was used for the research described in the article.

Appendix

A.1. Abbreviations

This is the list of abbreviations used in the mathematical model of PEMFC

C Concentration
D Diffusion coefficient (m^2/s)
F Faradays constant (96485 C mol^{-1})
E Nernst voltage of a PEMFC (V)
M Molar mass (g/mol)
P Pressure (Pa)
i Stack current density (A/m^2)

Table A.3
Parameters involved in Compressor model.

Parameter	Value	Parameter	Value
θ	$T_{cp,in}/298$	δ	$p_{cp,in}/1$
C_p	1004	J_{cp}	5×10^{-5}
d_c	0.2286	η_{cm}	1
β	14	η_{cp}	0.775
γ	1.4	$T_{cp,in}$	T_{atm}
ρ_a	1.23	T_{atm}	298
$p_{cp,in}$	p_{atm}	p_{atm}	101325

Table A.4
Parameters involved in Anode Channel.

Parameter	Value
M_v	18.02×10^{-3}
M_{H_2}	2.016×10^{-3}
R_{H_2}	4124.3
R_v	461.5
V_{an}	0.005

Table A.5
Parameters involved in the supply manifold.

Parameter	Value
R_a	2.869×10^{2}
V_{sm}	0.02
γ	1.4
$K_{sm,out}$	0.36×10^{-5}

I Current (A)
J Inertia (kg/m^2)
γ Specific heat ratio (J/(kg K))
K Restriction constant
n Number of fuel cells in stack
u Control input
λ Water content

A.2. Subscripts

These are used as the subscripts of the main nomenclatures
an Anode
ca Cathode
w Water
a Air
H_2 Hydrogen
O_2 Oxygen
m Membrane
st Stack
cp Compressor motor
out Output/Exiting
hum Humidifier air
v Water vapor *net* Total
react Consumed in reaction
rm Return manifold
amb Ambient
N_2 Nitrogen
sat Saturation
sm Supply manifold
in Entering/input
ref Reference

A.3. Model parameters

See Tables A.3–A.8.

Table A.6
Parameters involved in Cathode Channel.

Parameter	Value
$y_{O_{2,ca,in}}$	0.21
M_{O_2}	32×10^{-3}
M_{N_2}	28×10^{-3}
M_v	18.02×10^{-3}
R_{O_2}	259.8
R_{N_2}	296.8
R_v	461.5
V_{ca}	0.01
$K_{ca,out}$	0.2177×10^{-5}
n	381
F	96485

Table A.7
Parameters involved in Anode Channel.

Parameter	Value
M_v	18.02×10^{-3}
M_{H_2}	2.016×10^{-3}
R_{H_2}	4124.3
R_v	461.5
V_{an}	0.005

Table A.8
Parameters involved in Stack Voltage Model.

Parameter	Value
c_1	10
t_m	0.0125
b_2	350
i_{max}	2.2
c_3	2

References

[1] Ovaere M, Proost S. Cost-effective reduction of fossil energy use in the European transport sector: An assessment of the fit for 55 package. Energy Policy 2022;168:113085.

[2] Esfe MH, Arani AAA, Esfandeh S, Afrand M. Proposing new hybrid nano-engine oil for lubrication of internal combustion engines: Preventing cold start engine damages and saving energy. Energy 2019;170:228–38.

[3] Amigues J-P, Moreaux M. Competing land uses and fossil fuel, and optimal energy conversion rates during the transition toward a green economy under a pollution stock constraint. J Environ Econ Manag 2019;97:92–115.

[4] Al-Aboosi FY, El-Halwagi MM, Moore M, Nielsen RB. Renewable ammonia as an alternative fuel for the shipping industry. Curr Opin Chem Eng 2021;31:100670.

[5] Thounthong P, Mungporn P, Guilbert D, Takorabet N, Pierfederici S, Nahid-Mobarakeh B, et al. Design and control of multiphase interleaved boost converters-based on differential flatness theory for PEM fuel cell multi-stack applications. Int J Electr Power Energy Syst 2021;124:106346.

[6] Lü X, Qu Y, Wang Y, Qin C, Liu G. A comprehensive review on hybrid power system for PEMFC-HEV: Issues and strategies. Energy Convers Manage 2018;171:1273–91.

[7] Fan J, Chen M, Zhao Z, Zhang Z, Ye S, Xu S, et al. Bridging the gap between highly active oxygen reduction reaction catalysts and effective catalyst layers for proton exchange membrane fuel cells. Nat Energy 2021;6(5):475–86.

[8] Alaswad A, Omran A, Sodre JR, Wilberforce T, Pignatelli G, Dassisti M, et al. Technical and commercial challenges of proton-exchange membrane (PEM) fuel cells. Energies 2021;14(1):144.

[9] Olabi A, Wilberforce T, Abdelkareem MA. Fuel cell application in the automotive industry and future perspective. Energy 2021;214:118955.

[10] Fink C, Gößling S, Karpenko-Jereb L, Urthaler P. CFD simulation of an industrial PEM fuel cell with local degradation effects. Fuel Cells 2020;20(4):431–52.

[11] Xu Y, Zheng B, Song K, Zhang K, Fang R. Non-Fourier heat conduction and thermal-stress analysis of a spherical ice particle subjected to thermal shock in PEM fuel cell at quick cold start-up. J Energy Eng 2021;147(5):04021028.

[12] Fan L, Xing L, Tu Z, Chan SH. A breakthrough hydrogen and oxygen utilization in a H2-O2 PEMFC stack with dead-ended anode and cathode. Energy Convers Manage 2021;243:114404.

[13] Al-Othman A, Nancarrow P, Tawalbeh M, Ka'ki A, El-Ahwal K, El Taher B, et al. Novel composite membrane based on zirconium phosphate-ionic liquids for high temperature PEM fuel cells. Int J Hydrogen Energy 2021;46(8):6100–9.

[14] Cao Y, Kou X, Wu Y, Jermsittiparsert K, Yildizbasi A. PEM fuel cells model parameter identification based on a new improved fluid search optimization algorithm. Energy Rep 2020;6:813–23.

[15] Xingying B, Lizhong L, Huang B, Jian Q, Cheng Z. Performance improvement of proton exchange membrane fuel cell stack by dual-path hydrogen supply. Energy 2022;123297.

[16] Gómez JC, Serra M, Husar A. Controller design for polymer electrolyte membrane fuel cell systems for automotive applications. Int J Hydrogen Energy 2021.

[17] Won J, Oh H, Hong J, Kim M, Lee W-Y, Choi Y-Y, et al. Hybrid diagnosis method for initial faults of air supply systems in proton exchange membrane fuel cells. Renew Energy 2021;180:343–52.

[18] Tang X, Wang C, Hu Y, Liu Z, Li F. Adaptive fuzzy PID based on granular function for proton exchange membrane fuel cell oxygen excess ratio control. Energies 2021;14(4):1140.

[19] Cruz Rojas A, Lopez Lopez G, Gomez-Aguilar J, Alvarado VM, Sandoval Torres CL. Control of the air supply subsystem in a PEMFC with balance of plant simulation. Sustainability 2017;9(1):73.

[20] Taing E, Lee E, West J, Ok J. Control of a third-order PEMFC.

[21] Deng Z, Chen Q, Zhang L, Fu Z. Data driven NARMAX modeling for PEMFC air compressor. Int J Hydrogen Energy 2020;45(39):20321–8.

[22] Park G, Gajic Z. A simple sliding mode controller of a fifth-order nonlinear PEM fuel cell model. IEEE Trans Energy Convers 2013;29(1):65–71.

[23] Xia L, Zhao D, Li F, Wang X, Meng J. Research on control method of PEMFC cathode oxygen excess ratio. Xibei Gongye Daxue Xuebao/J Northwest Polytech Univ 2020;38(5):987–93.

[24] Grujicic M, Chittajallu K, Law E, Pukrushpan J. Model-based control strategies in the dynamic interaction of air supply and fuel cell. Proc Inst Mech Eng A 2004;218(7):487–99.

[25] Derbeli M, Charaabi A, Barambones O, Napole C. High-performance tracking for proton exchange membrane fuel cell system PEMFC using model predictive control. Mathematics 2021;9(11):1158.

[26] Liu J, Gao Y, Yin Y, Wang J, Luo W, Sun G. Sliding mode control of PEMFC systems. In: Sliding mode control methodology in the applications of industrial power systems. Springer; 2020, p. 83–102.

[27] Silaa MY, Derbeli M, Barambones O, Cheknane A. Design and implementation of high order sliding mode control for PEMFC power system. Energies 2020;13(17):4317.

[28] Nouira H, Hammami S, El-Amraoui A, Goncalves G, Bouchriha H. Periodic vehicle routing problem for home HemoDialysis care. In: 2019 international conference on industrial engineering and systems management. IEEE; 2019, p. 1–6.

[29] Abbaker AO, Wang H, Tian Y. Robust model-free adaptive interval type-2 fuzzy sliding mode control for PEMFC system using disturbance observer. Int J Fuzzy Syst 2020;22(7):2188–203.

[30] Souissi A. Adaptive sliding mode control of a PEM fuel cell system based on the super twisting algorithm. Energy Rep 2021;7:3390–9.

[31] Tvoroshenko I, Ahmad MA, Mustafa SK, Lyashenko V, Alharbi AR. Modification of models intensive development ontologies by fuzzy logic. WARSE; 2020.

[32] Maksymenko A. Development of control system for waste pyrolysis unit of agricultural complex with the application of fuzzy logic. Technol Audit Product Reserves 2021;4(2 (60)):16–21.

[33] Sharkawy A-N. Principle of neural network and its main types. J Adv Appl Comput Math 2020;7:8–19.

[34] Piffard M, Gerard M, Bideaux E, Da Fonseca R, Massioni P. Control by state observer of PEMFC anodic purges in dead-end operating mode. IFAC-PapersOnLine 2015;48(15):237–43.

[35] Xu L, Hu Z, Fang C, Li J, Hong P, Jiang H, et al. Anode state observation of polymer electrolyte membrane fuel cell based on unscented Kalman filter and relative humidity sensor before flooding. Renew Energy 2021;168:1294–307.

[36] Dali A, Abdelmalek S, Bakdi A, Bettayeb M. A novel effective nonlinear state observer based robust nonlinear sliding mode controller for a 6 kW proton exchange membrane fuel cell voltage regulation. Sustain Energy Technol Assess 2021;44:100996.

[37] Cecilia A, Serra M, Costa-Castelló R. PEMFC state and parameter estimation through a high-gain based adaptive observer. IFAC-PapersOnLine 2020;53(2):5895–900.

[38] Cruz-Zavala E, Moreno JA, Fridman LM. Uniform robust exact differentiator. IEEE Trans Automat Control 2011;56(11):2727–33.

[39] Reichhartinger M, Spurgeon S, Forstinger M, Wipfler M. A robust exact differentiator toolbox for matlab®/simulink®. IFAC-PapersOnLine 2017;50(1):1711–6.

[40] Harms C, Köhrmann F, Dyck A. Study of the influence of key test parameters on the performance of a PEMFC stack. Solid State Ion 2015;275:75–9.

[41] Wilberforce T, Biswas M, Omran A. Power and voltage modelling of a proton-exchange membrane fuel cell using artificial neural networks. Energies 2022;15(15):5587.

[42] Deng S, Zhang J, Zhang C, Luo M, Ni M, Li Y, Zeng T. Prediction and optimization of gas distribution quality for high-temperature PEMFC based on data-driven surrogate model. Appl Energy 2022;327:120000.

[43] Tan J, Hu H, Liu S, Chen C, Xuan D. Optimization of PEMFC system operating conditions based on neural network and PSO to achieve the best system performance. Int J Hydrogen Energy 2022;47(84):35790–809.

[44] Chen X, Xu J, Fang Y, Li W, Ding Y, Wan Z, et al. Temperature and humidity management of PEM fuel cell power system using multi-input and multi-output fuzzy method. Appl Therm Eng 2022;203:117865.
[45] Dumlu A, Kaleli A, Erentürk K, Ayten KK. Model-based sliding mode control technique for the stewart platform mechanism. In: 2017 international conference on engineering and technology. IEEE; 2017, p. 1–5.
[46] Javaid U, Mehmood A, Arshad A, Imtiaz F, Iqbal J. Operational efficiency improvement of PEM fuel cell—A sliding mode based modern control approach. IEEE Access 2020;8:95823–31.
[47] Javaid U, Iqbal J, Mehmood A, Uppal AA. Performance improvement in polymer electrolytic membrane fuel cell based on nonlinear control strategies—A comprehensive study. PLoS One 2022;17(2):e0264205.
[48] Carnes B, Spernjak D, Luo G, Hao L, Chen KS, Wang C-Y, et al. Validation of a two-phase multidimensional polymer electrolyte membrane fuel cell computational model using current distribution measurements. J Power Sources 2013;236:126–37.
[49] Carnes B, Chen KS, Hao L, Luo G, Ji Y, Wang C-Y, et al. Validation and uncertainty quantification of a two-phase, multidimensional PEMFC computer model using high-resolution segmented current collector data. In: International conference on fuel cell science, engineering and technology, Vol. 54693. 2011, p. 773–9.
[50] Wang Y, Wang Y, Xu J, Chai T. Observer-based discrete adaptive neural network control for automotive PEMFC air-feed subsystem. IEEE Trans Veh Technol 2021;70(4):3149–63.
[51] Hu D, Wang Y, Li J, Yang Q, Wang J. Investigation of optimal operating temperature for the PEMFC and its tracking control for energy saving in vehicle applications. Energy Convers Manage 2021;249:114842.
[52] Puranik SV, Keyhani A, Khorrami F. State-space modeling of proton exchange membrane fuel cell. IEEE Trans Energy Convers 2010;25(3):804–13.
[53] She Y, Baran ME, She X. Multiobjective control of PEM fuel cell system with improved durability. IEEE Trans Sustain Energy 2012;4(1):127–35.
[54] İnci M. A flexible perturb & observe MPPT method to prevent surplus energy for grid-failure conditions of fuel cells. Int J Hydrogen Energy 2021;46(79):39483–98.
[55] Savrun MM, İnci M, Büyük M. Design and analysis of a high energy efficient multi-port DC-DC converter interface for fuel cell/battery electric vehicle-to-home (V2H) system. J Energy Storage 2022;45:103755.
[56] Vahidi A, Stefanopoulou A, Peng H. Current management in a hybrid fuel cell power system: A model-predictive control approach. IEEE Trans Control Syst Technol 2006;14(6):1047–57.
[57] Pukrushpan JT, Stefanopoulou AG, Peng H. Control of fuel cell breathing. IEEE Control Syst Mag 2004;24(2):30–46.
[58] Ullah S, Khan Q, Mehmood A, Kirmani SAM, Mechali O. Neuro-adaptive fast integral terminal sliding mode control design with variable gain robust exact differentiator for under-actuated quadcopter UAV. ISA Trans 2022;120:293–304.